JOURNAL OF GEOPHYSICAL RESEARCH, VOL. 115, B03402, doi:10.1029/2009JB006515, 2010

Savage-Hutter model for avalanche dynamics in inclined channels: Analytical solutions

Narcisse Zahibo,[1] Efim Pelinovsky,[1,2] Tatiana Talipova,[1,2] and Irina Nikolkina[1,3]

Received 3 April 2009; revised 17 November 2009; accepted 10 December 2009; published 2 March 2010.

[1] The Savage-Hutter model is applied to describe gravity driven shallow water flows in inclined channels of parabolic-like shapes modeling avalanches moving in mountain valleys or landslide motions in underwater canyons. The Coulomb (sliding) friction term is included in the model. Several analytical solutions describing the nonlinear dynamics of avalanches are obtained: the nonlinear deformed (Riemann) wave, the dam break problem, self-similar solutions and others. Some of them extend the known solution for an inclined plate (one-dimensional geometry). The cross-section shape of the inclined channels significantly influences the speed of avalanche propagation and characteristic time of dynamical processes. Obtained analytical solutions can be used to test numerical models and to give insights into the structure of avalanche flow and to highlight basic mechanisms of avalanche dynamics.

Citation: Zahibo, N., E. Pelinovsky, T. Talipova, and I. Nikolkina (2010), Savage-Hutter model for avalanche dynamics in inclined channels: Analytical solutions, *J. Geophys. Res.*, *115*, B03402, doi:10.1029/2009JB006515.

1. Introduction

[2] Gravitational flows like submarine and aerial landslides, debris avalanches and pyroclastic flows from volcanoes are frequently reported as the sources of tsunami waves. In 1958, such an avalanche from Fairweather Mountain induced a huge swash of 524 m on the opposite side of the Lituya bay, Alaska, and tsunami waves reached 21 m near the bay entrance [*Miller*, 1960]. The pyroclastic flows were generated several times on Montserrat Island (the Lesser Antilles, Caribbean) due to continual volcano activity and caused three tsunami events recorded in Guadeloupe and Montserrat in the last decade [*Heinrich et al.*, 1998; *Mangeney et al.*, 2000a; *Pelinovsky et al.*, 2004; *Zahibo et al.*, 2008b]. The various analytical and numerical models are developed to describe tsunamis generated by landslides. In many studies [*Pelinovsky and Poplavsky*, 1996; *Watts*, 2000; *Tinti et al.*, 2001; *Liu et al.*, 2003; *Pelinovsky*, 2003; *Sammarco and Renzi*, 2008], the landslide is assumed as a solid block moving under the joint action of gravity, the Coulomb friction and hydraulic resistance in turbulent flow. More realistic models of tsunami generation include the "two-layer" approach which jointly describes tsunami wave and a landslide propagation influencing one another [*Imamura and Gica*, 1996; *Assier-Rzadkiewicz et al.*, 2000; *Mangeney et al.*, 2000a; *Heinrich et al.*, 1999, 2001; *Bouchut et al.*, 2003; *Fine et al.*, 2003, 2005; *Mangeney-Castelnau et al.*, 2003, 2005; *Le Friant et al.*, 2006; *Fernandez-Nieto et al.*, 2008]. Some attempts have been made to simulate submarine landslides using the full three-dimensional (3-D) Navier-Stokes equations [*Heinrich et al.*, 1998, 1999; *Mangeney et al.*, 2000b]. Similar models developed to describe dry subaerial avalanches, pyroclastic and debris flows including possible sources of tsunami, have aroused much interest in the last decade [see also *Gray et al.*, 1999; *Mangeney et al.*, 2000b; *Heinrich et al.*, 2001; *Bouchut et al.*, 2003; *Mangeney-Castelnau et al.*, 2003, 2005; *Le Friant et al.*, 2006; *Fernandez-Feria*, 2006; *Rudenko et al.*, 2007; *Mangeney et al.*, 2007a; *Bouchut et al.*, 2008; *Pirulli and Mangeney*, 2008; *Pelanti et al.*, 2008; *Yu et al.*, 2009; *Luca et al.*, 2009]. Most of such models of landslides and avalanches are based on homogeneous shallow water flows that are deformed during propagation. These models use various approximations of the vertical structure of the velocity field (uniform as in the ideal fluid, or parabolic as for a viscous fluid), as well as different approximations of the friction law (the Coulomb friction, Bagnold behavior, Pouliquen law); the derivation of the mentioned models can be found in the recently published book by *Pudasaini and Hutter* [2007]. Although most of these models are realized in numerical codes and are applied for modeling real and prognostic events, analytical solutions can be used to test numerical models and to gain insights into the structure of avalanche flow, and to highlight basic mechanisms of avalanche dynamics.

[3] In this paper special attention is paid to the analytical description of dry subaerial avalanche dynamics basing on the Savage-Hutter model. The number of the analytical solutions of the gravity driven shallow water flow is limited. *Savage and Hutter* [1989, 1991] constructed some self-similar solutions called parabolic cap and M waves due to their shapes; see also the book by *Pudasaini and Hutter*

[1]Physics Department, University of the French West Indies and Guiana, Pointe-à-Pitre, Guadeloupe.
[2]Department of Nonlinear Geophysical Processes, Institute of Applied Physics, Nizhny Novgorod, Russia.
[3]Department of Applied Mathematics, Nizhny Novgorod State Technical University, Nizhny Novgorod, Russia.

0148-0227/10/2009JB006515$09.00

Figure 1. The 2 December 2008 pyroclastic surge effects on St. George's Hill, Montserrat (see http://www.mvo.ms).

[2007]. *Mangeney et al.* [2000b] found the analytical solution to a one-dimensional dam break problem over inclined plane also taking into account the Coulomb friction. It was widely used to test the debris avalanche numerical models applied to evaluate the hazard of the volcano eruption in the Lesser Antilles [*Heinrich et al.*, 1999, 2001; *Mangeney et al.*, 2000a; *Le Friant et al.*, 2003, 2006]. *Fernandez-Feria* [2006] extended this analysis to arbitrary bottom slopes; the axisymmetric dam break problem is solved by *Kerswell* [2005]. *Rudenko et al.* [2007] found the exact solution that represented the nonlinear deformed wave in an ideal flow (neglected friction) along a plate of a constant slope.

[4] The model we used here includes sliding friction (the Coulomb law). Although the simple friction law suggests simplified behavior of the flow which is expected to be different from the natural one, some basic mechanisms can be deduced. For instance, natural avalanches are submitted to erosion processes that can significantly change their dynamics and generate surge waves [*Mangeney et al.*, 2007b]. Furthermore the fluid phase generally plays a significant role as described, for example, by *Pelanti et al.* [2008]. It must be said that the simple model based on Coulomb friction is very convenient to predict potential events and to analyze historical events because it contains only one empirical parameter (friction angle) as pointed out by *Pirulli and Mangeney* [2008]. That is why this kind of friction is used in our study.

[5] Analytical solutions of the gravity driven shallow water flow with Coulomb friction are obtained in the literature for 1-D geometry only. However, gravity driven masses move in basins of more complicated geometry. As a rule, they move in inclined channels (valleys on mountains and submarine canyons) which are generally diverging, converging or twisted in various parts. Some of them have straight parabolic-like shapes at least in a part of flank (Figure 1). We provide here several new analytical solutions for gravity driven shallow water flow in inclined channels of constant slope with the specific parabolic-like cross section. New effects in the avalanche dynamics comparable to those known for the 1-D avalanche motion along an inclined plate are related with the parabolic-like cross-section shape of the channel which influence the speed of avalanche propagation and characteristic time of dynamical processes.

[6] The paper is organized as follows. The basic model to describe the avalanche motion that represents the gravity driven shallow water flow (simplified Savage-Hutter model) in a narrow inclined channel of parabolic-like cross section is given in section 2. Nonlinear deformation of the avalanche shape for the nonzero sign constant initial distribution of the particle velocity in the avalanche body is studied in section 3. The dam break problem for gravity driven flow in an inclined channel with initial zero velocity distribution is investigated in section 4; it is the extension of the well-known 1-D solution described by *Stoker* [1957] and *Mangeney et al.* [2000b]. Other self-similar solutions for the avalanche of finite length and symmetrical shape in the inclined channels are also found in section 4; they are extensions of the M wave and parabolic cap solutions for the 1-D avalanche given by *Pudasaini and Hutter* [2007]. The analytical solution for an avalanche initially at rest in a parabolic channel is obtained in section 5; from a mathematical point of view it is the extension of the Carrier-Greenspan transformation [*Carrier and Greenspan*, 1958] used early in the theory of water waves in particular tsunami waves [*Zahibo et al.*, 2006; *Choi et al.*, 2008]. The discussion of obtained results is given in the conclusion.

2. Basic Model of the Gravity Driven Shallow Water Flow

[7] To describe the gravity driven flow (debris avalanche or submarine landslide) we follow *Pudasaini and Hutter* [2007] using the two-dimensional depth-integrated shallow water equations for the incompressible fluid with the Coulomb-type friction term (Savage-Hutter model); the earth pressure coefficients in the Savage-Hutter model have been set to 1. This model as pointed above [*Pirulli and Mangeney*, 2008] is very convenient to predict potential events and also to analyze historical events because it contains only one empirical parameter (friction angle). In the system of coordinates linked to the topography the equations of mass and momentum conservation have the following form [see *Mangeney et al.*, 2000b]:

$$\frac{\partial h}{\partial t}+\frac{\partial}{\partial x}(hu)+\frac{\partial}{\partial y}(hw)=0, \tag{1}$$

$$\frac{\partial u}{\partial t}+u\frac{\partial u}{\partial x}+w\frac{\partial u}{\partial y}+g\cos\theta\frac{\partial h}{\partial x}=g\sin\theta_x-\mu g\cos\theta\frac{u}{\sqrt{u^2+w^2}}, \tag{2}$$

$$\frac{\partial w}{\partial t}+u\frac{\partial w}{\partial x}+w\frac{\partial w}{\partial y}+g\cos\theta\frac{\partial h}{\partial y}=g\sin\theta_y-\mu g\cos\theta\frac{w}{\sqrt{u^2+w^2}}, \tag{3}$$

where

x, y local slope and parallel coordinates, m;
$h(x, y, t)$ flow height perpendicular to the local slope, m;

u, w depth-averaged velocities along x and y axes, respectively, m/s;
g acceleration due to gravity, m/s^2;
θ steepest slope angle, deg;
θ_x, θ_y slope angles along x and y axes, deg;
$\mu = \tan(\varphi)$ sliding friction coefficient, nondimension;
φ dynamic friction angle, deg.

[8] The value of φ depends on the landslide material, and it has not been studied well. Usually it is considered to be relatively small for sand-textured debris (17–30° [*Heinrich et al.*, 2001]) and relatively large for a granular debris avalanche (20–40° [*Le Friant et al.*, 2003]). Very often this angle is estimated using comparison between the observed data and the results of numerical modeling. In particular, for the debris avalanche on the Montserrat volcano the dynamic friction angle is tested in a wide range as 13–35° and for the simple friction law the value 13–14.5° has been chosen. [*Voight et al.*, 2002; *Heinrich et al.*, 2001]. *Le Friant et al.* [2003] state that this angle for the flank collapse event on the Montagne Pelée, Martinique, has been estimated as 6.6° from observations and has been taken about 7° for numerical simulations.

[9] The given equations are simplified compared to the advanced version of the Savage-Hutter models of complex topography recently proposed by *Bouchut and Westdickenberg* [2004] and *Mangeney et al.* [2007a]. We would like to point out that the given equations differ from the well-known "fluid" shallow water system in the friction term, which is usually proportional to $u|u|$ (Chezy friction); this Saint Venant model is also used in avalanche dynamics [*Bouchut et al.*, 2003; *Mangeney-Castelnau et al.*, 2003, 2005]. In fact, it is rather complicated to describe and to parameterize the dissipative processes in landslides and avalanches, and various formulas are applied in practice [see *Pudasaini and Hutter*, 2007]. Meanwhile, the Coulomb-type friction has only one empirical parameter (friction angle, φ) and as mentioned above, this model is very convenient to predict potential events and also to analyze historical events [see *Pirulli and Mangeney*, 2008]. Here we use Coulomb-type friction in order to obtain analytical solutions of equations (1)–(3).

[10] Avalanches and landslides usually move in narrow channels (valleys and canyons), see for instance Figure 1. Assuming that the channel axis is straight and the flow is almost uniform in the cross section, the shallow water equations may be integrated on the cross section and effective 1-D system may be derived (typical approach for river hydraulics). This procedure is demonstrated quite extensively by *Pudasaini and Hutter* [2007] and yields

$$\frac{\partial S}{\partial t} + \frac{\partial}{\partial x}(Su) = 0, \tag{4}$$

$$\frac{\partial u}{\partial t} + u\frac{\partial u}{\partial x} + g\cos\theta\frac{\partial h}{\partial x} = g\sin\theta - \mu g\cos\theta\ \mathrm{sgn}\ u, \tag{5}$$

where $S(x, t)$ area of the cross section of the channel, m^2; $h(x, t)$ avalanche height along x axis of channel, m; and $u(x, t)$ mean velocity flow, m/s. To close this system, the function $S(h)$ which is given as an integral expression over the width of a channel should be determined. If the cross section has a parabolic-like shape,

$$z(y) = k|y|^m, \tag{6}$$

with positive arbitrary constants, k and m (Figure 2), the function S is

$$S = \frac{2m}{(m+1)k^{1/m}}h^{(m+1)/m}. \tag{7}$$

As a result, equation (4) transforms to

$$\frac{\partial h}{\partial t} + u\frac{\partial h}{\partial x} + \frac{m}{m+1}h\frac{\partial u}{\partial x} = 0, \tag{8}$$

and the system of equations (5) and (8) becomes closed. It differs from the "classical" one-dimensional equations of the simplified Savage-Hutter model in the constant coefficient $m/(m+1)$, and may be transformed to them as $m \to \infty$ ($S \sim h$).

[11] Below we assume the constant slope of the inclined channel, θ, which should be relatively high ($\theta > \varphi$) to provide the gravity driven motion of the landslide. In this case $u > 0$ throughout and equation (5) is simplified to

$$\frac{\partial u}{\partial t} + u\frac{\partial u}{\partial x} + g\cos\theta\frac{\partial h}{\partial x} = g\sin\theta - \mu g\cos\theta. \tag{9}$$

[12] The basic system of the gravity driven flow, (8) and (9), is analyzed below. Mathematically, it is a hyperbolic system with constant coefficients and as for water waves above inclined bottom [*Stoker*, 1957; *Carrier and Greenspan*, 1958; *Zahibo et al.*, 2006; *Choi et al.*, 2008]; the Riemann invariants can be found explicitly

$$I_\pm = u \pm 2\sqrt{\frac{m+1}{m}gh\cos\theta} - g\alpha t, \tag{10}$$

where

$$\alpha = \sin\theta - \mu\cos\theta > 0, \tag{11}$$

and the system (8)–(9) can be rewritten in the form

$$\frac{\partial I_\pm}{\partial t} + c_\pm\frac{\partial I_\pm}{\partial x} = 0, \tag{12}$$

where the characteristic speeds are

$$c_\pm = \frac{3m+2}{4(m+1)}I_\pm + \frac{m+2}{4(m+1)}I_\mp + g\alpha t. \tag{13}$$

It should be mentioned that equations (12) and (13) appear in the problems of long water wave run-up on the coast [*Stoker*, 1957; *Carrier and Greenspan*, 1958; *Zahibo et al.*, 2006; *Choi et al.*, 2008] but the main difference here is that the bottom slope is not small (as in "run-up problems") and the Coulomb-type friction is not neglected. Mathematically, the initial and boundary conditions for water waves and avalanche dynamics also differ. That is why the "avalanche

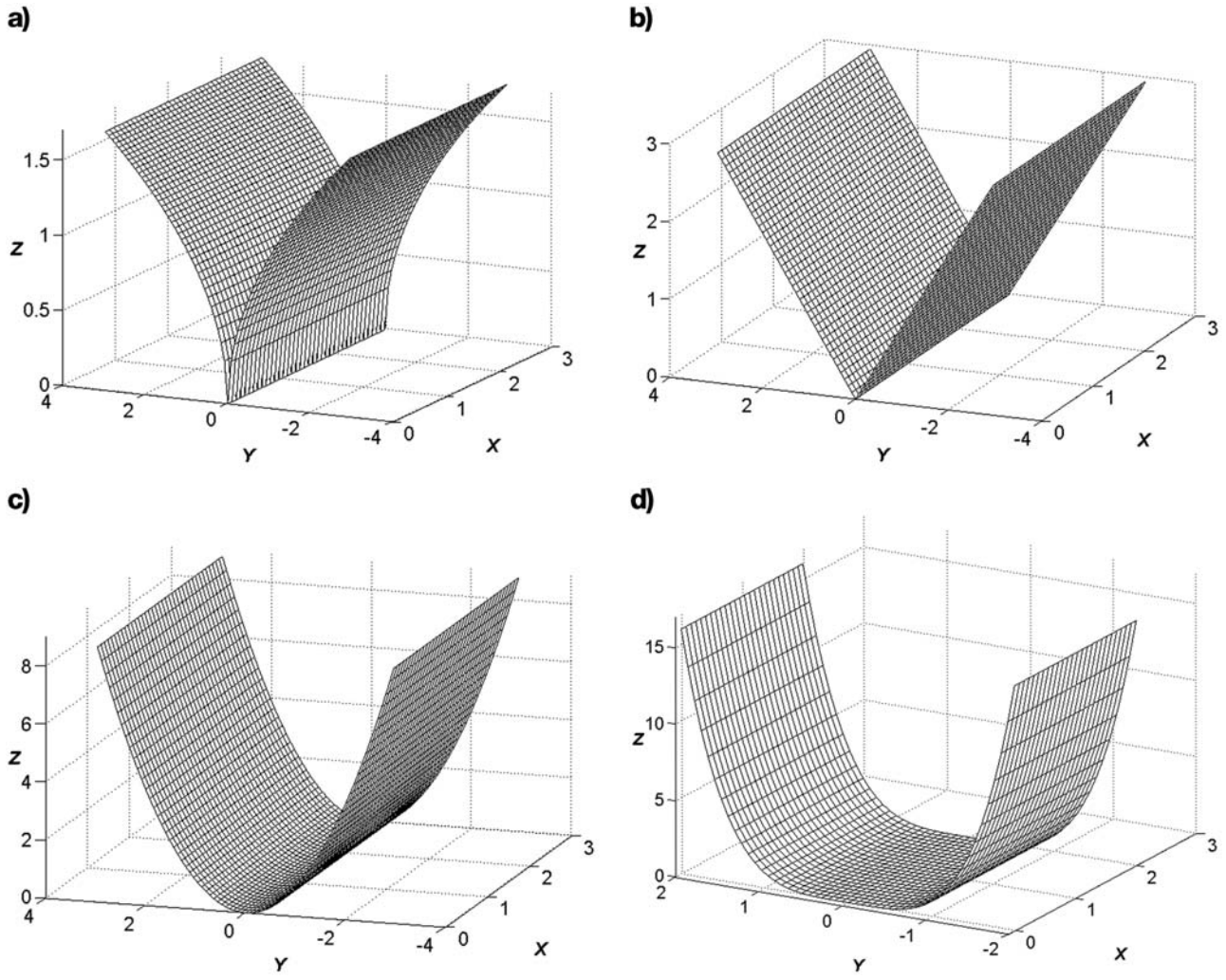

Figure 2. Different channel shapes of the cross channel: (a) m = 0.5, (b) m = 1, (c) m = 2, (d) m = 4.

solutions" cannot be directly obtained from the "water solutions." Physical variables, $h(x, t)$ and $u(x, t)$ are found from the algebraic equations (10) and the downslope component of the velocity field ($g\alpha t$) propagating under the action of the gravity force can be eliminated by use of

$$u(x,t) = g\alpha t + v(x,t), \tag{14}$$

$$v(x,t) = \frac{I_+ + I_-}{2}, \tag{15}$$

$$h = \frac{m}{16g\cos\theta(m+1)}(I_+ - I_-)^2, \tag{16}$$

where $\alpha > 0$ depends on the slope angle and friction coefficient, see (11). Another useful development is the change of coordinates, the accelerated reference system can be written as

$$X = x - \frac{g\alpha t^2}{2}, t = t. \tag{17}$$

As a result, system (12) is reduced to the nonlinear system with constant coefficients

$$\frac{\partial J_\pm}{\partial t} + C_\pm \frac{\partial J_\pm}{\partial X} = 0, \tag{18}$$

where the modified Riemann invariants $J_\pm$ are

$$J_\pm = v \pm 2\sqrt{\frac{m+1}{m} gh\cos\theta}, \tag{19}$$

and the modified characteristic speeds are

$$C_\pm = \frac{3m+2}{4(m+1)} J_\pm + \frac{m+2}{4(m+1)} J_\mp. \tag{20}$$

The system (18–20) now does not include the downslope component of the velocity field ($g\alpha t$). The new parameter m characterizing the cross section of the shape of the channel is added compared to the plane case. Equations (18)–(20)

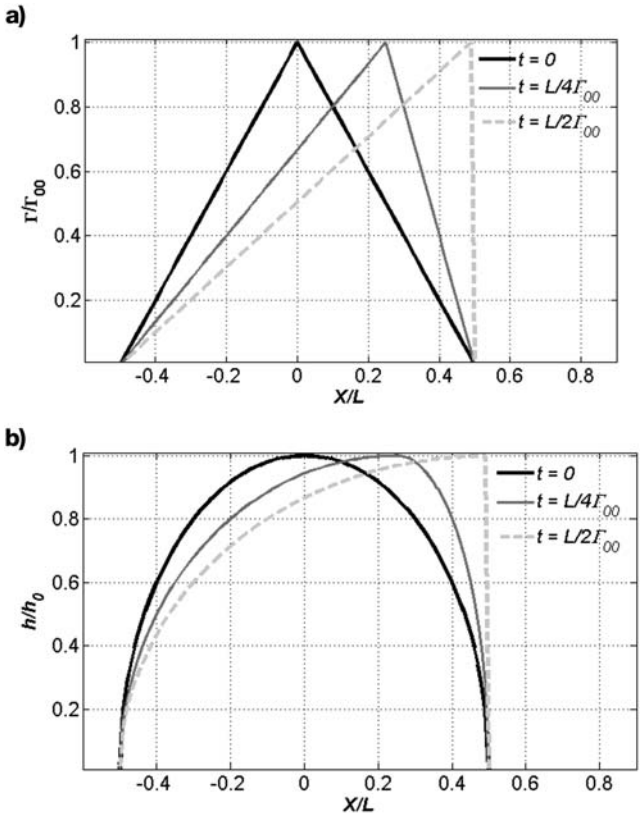

Figure 3. (a) Velocity and (b) height distributions in longitudinal direction for times 0, $L/4\Gamma_{00}$, and $L/2\Gamma_{00}$.

present the basic model of the avalanche motion in the inclined channel of parabolic-like cross section.

3. Nonlinear (Riemann) Wave Presentation of the Gravity Driven Flow

[13] A particular solution of the system (18) is $J_- = 0$, that leads to the following relation between the velocity and the flow height

$$v(x,t) = 2\sqrt{\frac{m+1}{m} g h \cos\theta}. \tag{21}$$

Using this solution equation (18) for J_+ can be reduced to the nonlinear PDE of the first order

$$\frac{\partial \Gamma}{\partial t} + \Gamma \frac{\partial \Gamma}{\partial X} = 0, \tag{22}$$

where

$$\Gamma = \frac{3m+2}{2(m+1)} v(X,t) \tag{23}$$

is the normalized velocity. The solution of (22) is expressed through the so-called Riemann wave [*Stoker*, 1957]

$$\Gamma(x,t) = \Gamma_0(X - \Gamma t), \tag{24}$$

where $\Gamma_0(X)$ describes the initial longitudinal landslide shape (exactly, $\sqrt{h_0(X)}$).

[14] The solution (24) in initial coordinates has the following evident physical meaning: the landslide moves with acceleration, $g\alpha$ (we consider the case when the gravity force is not balanced by Coulomb friction) and the shape of landslide deforms during the motion whereas the front steepness increases.

[15] The solution (24) has been obtained by *Rudenko et al.* [2007] for the particular case of free gravity flow (no friction) above an inclined plate ($m \to \infty$). Similar solutions have been studied for water waves above a horizontal bottom and in channels with parabolic-like cross section [*Pelinovsky and Troshina*, 1994; *Zahibo et al.*, 2008a]. Our solution includes both, the inclined channel of parabolic cross section and Coulomb friction.

[16] The nonlinear evolution of the avalanche body can be analyzed for any initial distribution of the height in the longitudinal direction and is illustrated here for a parabolic initial distribution of avalanche height. In this case the velocity distribution has triangular shape (as $\Gamma_0(X) \sim \sqrt{h_0(X)}$), with the initially equal front and back slopes, see Figure 3a. Analytically, the longitudinal evolution of the flow within the avalanche in the accelerated reference system (17) is described by

$$\frac{\Gamma(X,t)}{\Gamma_{00}} = \begin{cases} \dfrac{X + L/2}{\Gamma_{00} t + L/2} & -L/2 < X < \Gamma_{00} t \\ \dfrac{X - L/2}{\Gamma_{00} t - L/2} & \Gamma_{00} t < X < L/2, \end{cases} \tag{25}$$

where L is the avalanche length, and Γ_{00} is the maximum velocity in the center of the avalanche. In time, the steepness of the front slope increases, and the steepness of the back slope decreases

$$s(t) = \frac{s_0}{1 \mp s_0 t}, \tag{26}$$

where $s_0 = d\Gamma_0/dx$ is the initial steepness, and $\pm$ corresponds to the back/front slope. The longitudinal avalanche shape evolution is described by the following formula deducible from (25)

$$h(X,t) = h_0 \begin{cases} \left[1 - \dfrac{(X - \Gamma_{00} t)^2}{(-L/2 - \Gamma_{00} t)^2}\right] & -L/2 < X < \Gamma_{00} t \\ \left[1 - \dfrac{(X - \Gamma_{00} t)^2}{(L/2 - \Gamma_{00} t)^2}\right] & \Gamma_{00} t < X < L/2, \end{cases} \tag{27}$$

and is presented in Figure 3b.

[17] The given solutions are valid only for bounded times less than the breaking time

$$T_{br} = \frac{L}{2\Gamma_{00}} = \frac{L\sqrt{m(m+1)}}{2(3m+2)\sqrt{g h_0 \cos\theta}}, \tag{28}$$

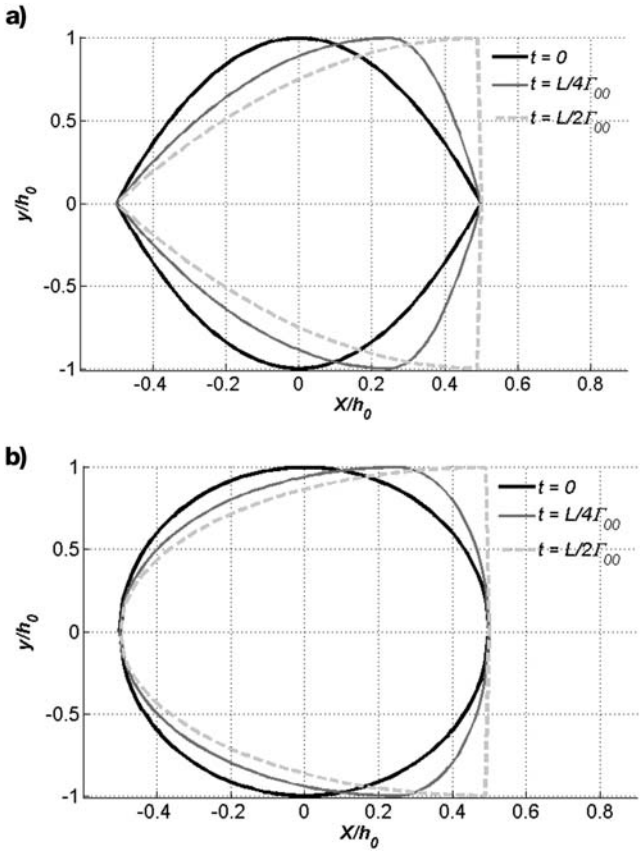

Figure 4. Avalanche contours for different times in the accelerated reference system for times 0, $\frac{L}{4\Gamma_{00}}$ and $\frac{L}{2\Gamma_{00}}$, (a) triangular channel ($m = 1$), (b) parabolic channel ($m = 2$).

when the avalanche front steepness is infinite. The breaking time depends on the slope angle and increases with the steepness of the slopes. It also depends on the cross section of the channel (parameter m) and decreases for narrow channels ($m \to 0$). We would like to mention that the breaking time does not depend on the friction coefficient, and the nonlinear deformation of the avalanche body in time is the same both for the friction and frictionless cases. However, the distance accomplished by an avalanche before breaking depends on friction.

[18] Let us investigate the influence of the cross section of an inclined channel on the evolution of the flow. It follows from (21) that the particle velocity increases when m decreases. For instance, for a channel of parabolic shape ($m = 2$) this speed is $(1.5)^{1/2} = 1.225$ times that on a plane slope, for the channel of triangle shape ($m = 1$) this factor is $2^{1/2} = 1.414$. As a result, an avalanche with the same height deforms quickly in narrow channels ($m \to 0$) and so, the flow is more energetic. The spatial structure of the deformed avalanche computed from (6) depends on the cross section of the channel (Figure 4). The avalanche rear tail in the channel of the triangular cross section is beak shaped, and in the parabolic channel it is parabolic like. In time the avalanche front becomes flattened in both cases. All the conclusions made above are valid for any initial distribution of the velocity (not only for triangles). In particular, equation (26) describes the time evolution of the maximum steepness of the avalanche longitudinal shape (in terms $d\Gamma/dx$), the breaking time is also determined definitely through the maximum value of $d\Gamma_0/dx$.

[19] After breaking, the avalanche profile becomes multivalued in the framework of the solution (24). Usually, multivalued solutions of hyperbolic equations are replaced by single-valued solutions with a discontinuity in height on the front to satisfy the approximation of the uniform distribution of the velocity along the depth of the shallow water model. Taking into account that the mass of the avalanche is conserved, the real configuration of the avalanche body with the shock front can be found from the multivalued solution using the law of "square equality." According to this approach which is popular in nonlinear waves [*Stoker*, 1957; *Whitham*, 1974] the front location is determined from the condition $S_1 = S_2$, as illustrated in Figure 5.

[20] The avalanche height h_L decreases in time, and its length increases so as to conserve the avalanche mass. For large times the height and the length of the avalanche satisfy the asymptotic expressions

$$X_{fr} \approx \sqrt{\frac{2L\Gamma_{00}t}{3}}, h_L \approx h_0\sqrt{\frac{8}{3\Gamma_{00}t}}. \quad (29)$$

As a result, the avalanche shape in the longitudinal direction being initially parabolic tends to a triangle.

[21] The formation of the shock profiles of the avalanche body should be obtained in various shallow water models of the avalanche due to their hyperbolicity; this process is specially investigated numerically in the framework of the two-phase model of the shallow granular flow [*Pelanti et al.*, 2008].

4. Self-Similar Solutions

[22] The famous self-similar analytical solution of the shallow water system is the dam break solution on the

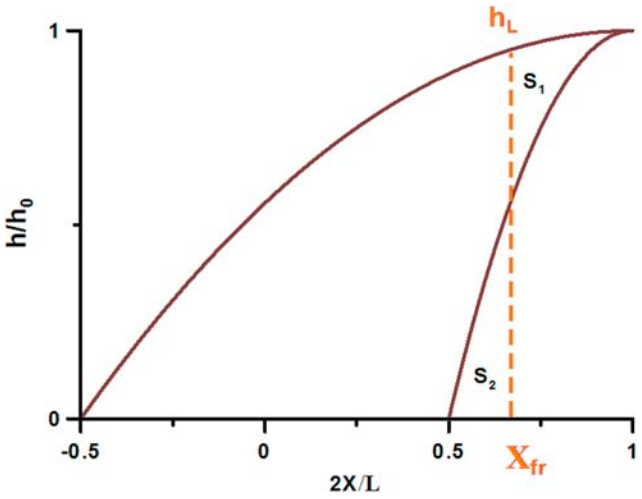

Figure 5. Avalanche shape after breaking in the longitudinal direction. The red line corresponds to the front location.

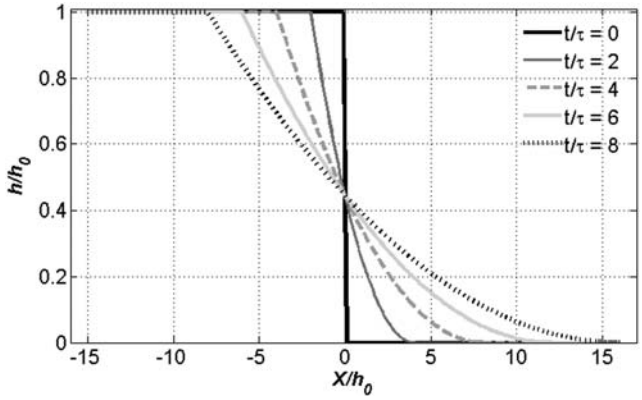

Figure 6. Avalanche shape evolution in the dam break problem for time slices with time increment $\tau = h_0/c_0$.

horizontal plane bottom described in the book by *Stoker* [1957]. This analysis was extended by *Mangeney et al.* [2000b] for the debris avalanche flow along an inclined plate. Our system of gravity-driven flow in an inclined channel of parabolic-like cross section (18) can be also reduced to equations studied by *Stoker* [1957].

[23] Let us introduce a new variable of the dimension of velocity rather than avalanche depth:

$$c = \sqrt{\frac{m+1}{m} g h \cos\theta}. \tag{30}$$

With it, equations (18) can be rewritten in the form

$$\frac{\partial}{\partial t}(v \pm 2c) + (v \pm c)\frac{\partial}{\partial X}(v \pm 2c) = 0, \tag{31}$$

which is exactly the same as the equations studied by *Stoker* [1957] and by *Mangeney et al.* [2000b].

[24] The initial condition ($t = 0$) for the dam break problem on the inclined channel is

$$u(x,0) = 0, h(x,0) = \begin{cases} h_0 & x < 0 \\ 0 & x > 0. \end{cases} \tag{32}$$

In the modified variables it is reduced to

$$v(X,0) = 0, c(X,0) = \begin{cases} c_0 & X < 0 \\ 0 & X > 0, \end{cases} \tag{33}$$

which is by *Stoker* [1957] as the initial condition for the dam break problem on the horizontal plane. This means that the analytical solution given in the cited book can be used to obtain the solution of the dam break problem for the avalanche in the inclined channel with Coulomb friction as it was first shown by *Mangeney et al.* [2000b] for 1-D geometry.

[25] The classical solution to the dam break problem on the horizontal plane obtained by *Stoker* [1957] has the following form

$$c(X,t) = \begin{cases} c_0 & X < -c_0 t \\ \frac{1}{3}\left(2c_0 - \frac{X}{t}\right) & -c_0 t < X < 2c_0 t \\ 0 & 2c_0 t < X, \end{cases} \tag{34}$$

$$v(X,t) = \begin{cases} 0 & X < -c_0 t \\ \frac{2}{3}\left(c_0 + \frac{X}{t}\right) & -c_0 t < X < 2c_0 t \\ 2c_0 & 2c_0 t < X. \end{cases} \tag{35}$$

The "front" edge point moves with the highest speed, $2c_0$, the "quiet region" has speed c_0; both variables v and c vary linearly in the transition zone.

[26] Returning to the dam break problem for the gravity-driven flow in the inclined channel, we may say that the cross section of the channel and its slope influence the speed of the dam break process through the relation between c_0 and h_0 as follows

$$c_0 = \sqrt{\frac{m+1}{m} g h_o \cos\theta}. \tag{36}$$

[27] The process of "dam breaking" of the avalanche of the same height, h_0, is intensified in narrow channels ($m \rightarrow 0$) and along gentle slopes. The bottom friction influences the acceleration of the avalanche (through the accelerated system of coordinates) but not the dam break process. The avalanche shape in the longitudinal direction is described by the formula

$$h(X,t) = \begin{cases} h_0 & X < -c_0 t \\ \frac{h_0}{9}\left(2 - \frac{X}{c_0 t}\right)^2 & -c_0 t < X < 2c_0 t \\ 0 & 2c_0 t < X, \end{cases} \tag{37}$$

which follows from (35). The evolution of the avalanche shape is demonstrated in Figure 6. It is clearly seen that the initial discontinuity is diluted in time and its front becomes smoother.

[28] Formally, the found solutions oppose each other: whereas the Riemann wave always breaks, the "dam break" front becomes gentler as time proceeds. The difference between the two solutions is connected with the value of the initial velocity that can be zero (dam break problem) and nonzero (the Riemann wave). In the dam break problem ≪back≫ particles drop behind, which leads to the front extension. In the other case the particles of high speed, located in the ≪back≫ of the landslide overrun slow moving particles in the front. Thus, the avalanche dynamics is sensitive to the initial conditions.

[29] Some extensions of the classical dam break problem for the avalanche on an inclined plate have been done. *Fernandez-Feria* [2006] extended the 1-D dam break solution to more complicated initial condition different from (32); the avalanche shape is not constant at $x < 0$. In fact, *Fernandez-Feria* [2006] found an analytical solution only in

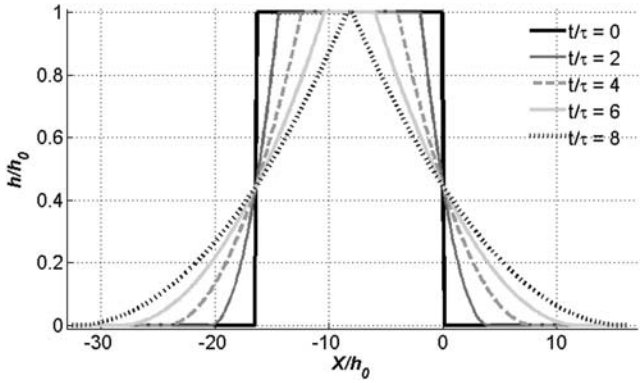

Figure 7. Avalanche shape evolution in the longitudinal direction for stepwise (rectangular) initial shape with increment $\tau = h_0/c_0$.

the vicinity of the avalanche edge, of which the motion does not depend on the avalanche shape behind the front, at least for small times. The detailed evolution of the avalanche shape has been obtained numerically in the cited paper. We would also like to point out a paper by *Mangeney-Castelnau et al.* [2005], where the detailed study of the spreading of the column of a frictional material has been investigated numerically. The scaling laws based on analytical solutions have been used successfully to reproduce experimental results on granular collapse. With the adequate scaling these solutions can be applied to analyze the avalanche evolution in the inclined channel.

[30] The solution of the dam break problem given above is one of the particular self-similar solutions of hyperbolic equations, and it is valid for a semi-infinity avalanche. If the avalanche has a table-top shape of total length L, both ends are evolving independently on the first stage according to the self-similar scenario. The dynamics of the front slope is described by (37), and the rear slope may be described by the following formula obtained from (37) by changing X to $-(X + L)$ and accordingly u to $-u$:

$$h(X,t) = \begin{cases} h_0 & X + L > c_0 t \\ \dfrac{h_0}{9}\left(2 + \dfrac{X+L}{c_0 t}\right)^2 & -2c_0 t < X + L < c_0 t \\ 0 & X + L < -2c_0 t. \end{cases} \quad (38)$$

[31] The evolution of the avalanche shape is shown in Figure 7 for $L/h_0 = 16.4$. The independent dynamics of the avalanche tails is valid for $t < L/c_0$, after that both tails influence each other and the landslide height decreases.

[32] The spatial structure of the avalanche computed with the use of (6) is shown in Figure 8. The avalanche edge is beak shaped in the channel of both, triangular and parabolic cross sections.

[33] If the initial avalanche length is relatively short, its shape evolution can be described by another kind of self-similar solutions. Such solutions (called parabolic cap and M wave) were found by *Savage and Hutter* [1989, 1991] and described by *Pudasaini and Hutter* [2007] for the avalanche along the inclined plane. The same solutions can be derived for avalanche dynamics in the inclined channel of parabolic-like cross section. It is again convenient to use the "accelerated" coordinates (17) and "reduced" velocity (15). In this case the basic equations (8) and (9) transform to

$$\frac{\partial h}{\partial t} + v\frac{\partial h}{\partial X} + \frac{m}{m+1}h\frac{\partial v}{\partial X} = 0, \quad (39)$$

$$\frac{\partial v}{\partial t} + v\frac{\partial v}{\partial X} + g\cos\theta\frac{\partial h}{\partial X} = 0. \quad (40)$$

[34] The self-similar solutions of this system are sought in the form

$$h(\xi,t) = \frac{1}{t^a}F(\xi), v(\xi,t) = \frac{1}{t^b}G(\xi), \xi = X/t^f, \quad (41)$$

where the functions F, G and the constants a, b, d should be determined. The first relation between the constants can be obtained from the avalanche mass conservation law (39) or from (4) and (7). This yields

$$\int_{-\infty}^{+\infty} h^{(m+1)/m}(X,t)dX = \text{const}, \quad (42)$$

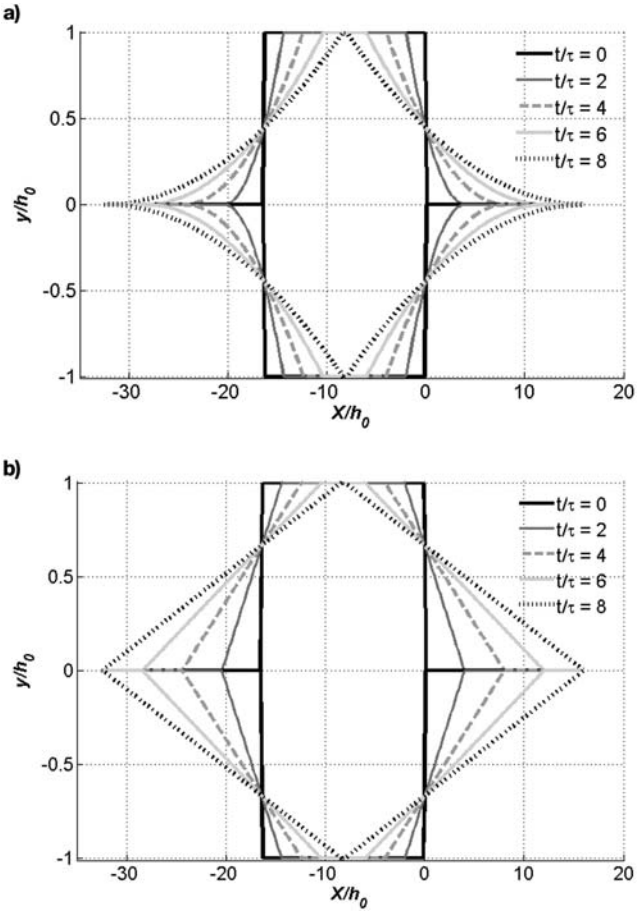

Figure 8. Avalanche contours in dam break problem: (a) channel of triangle cross section, and (b) channel of parabolic cross section, $\tau = h_0/c_0$.

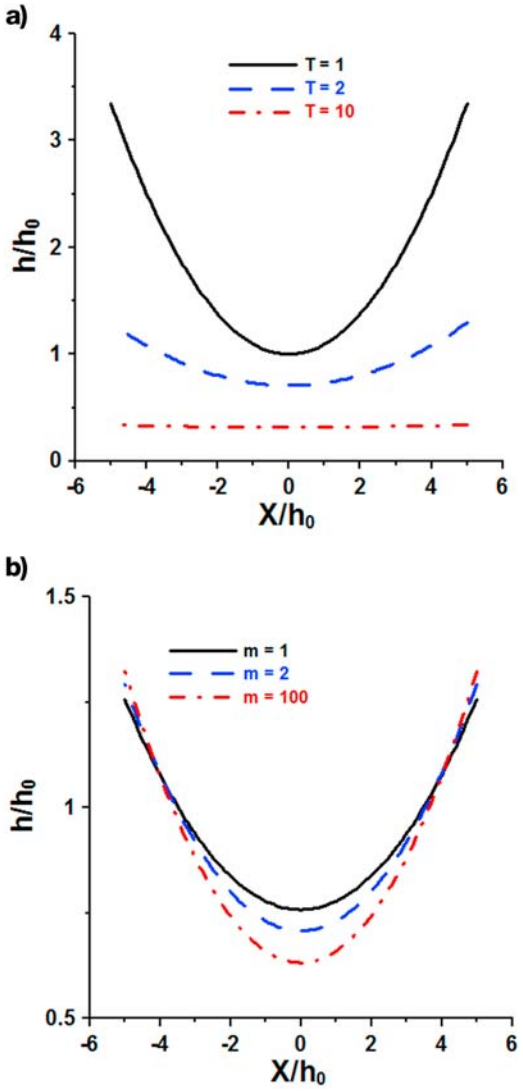

Figure 9. M wave avalanche shape in longitudinal direction (a) $m = 2$ (b) $T = 2$.

as well as

$$f = a\frac{m+1}{m}. \tag{43}$$

[35] After substitution of (41) in (39) and (40), these equations become

$$-aF - f\xi\frac{dF}{d\xi} + t^{-b-f+1}\left[G\frac{dF}{d\xi} + \frac{m}{m+1}F\frac{dG}{d\xi}\right] = 0 \tag{44}$$

$$-bG - f\xi\frac{dG}{d\xi} + t^{-b-f+1}G\frac{dG}{d\xi} + t^{-a-f+b+1}g\cos\theta\frac{dF}{d\xi} = 0. \tag{45}$$

Both equations would be ODEs when the time is not included. This argument leads to the algebraic equations for the coefficients, which are explicitly determined:

$$a = \frac{2m}{3m+2}, b = \frac{m}{3m+2}, f = \frac{2(m+1)}{3m+2}. \tag{46}$$

With these choices the resulting equation (44) can be integrated to yield

$$[-f\xi + G(\xi)]F^{\frac{m+1}{m}}(\xi) = \text{const}. \tag{47}$$

One of the solutions is chosen for the zero constant in (47), it determines the velocity

$$G(\xi) = \frac{2(m+1)}{3m+2}\xi. \tag{48}$$

With the use of (48) equation (45) is reduced to

$$g\cos\theta\frac{dF}{d\xi} = bf\xi, \tag{49}$$

and is easily integrated, with the result

$$F(\xi) = F_0 + \frac{m(m+1)}{g\cos\theta(3m+2)^2}\xi^2. \tag{50}$$

[36] The self-similar solution (41) expressed in the initial physical variables has the final form

$$\begin{aligned} h(\tilde{X},T) &= h_0\left[T^{-\frac{2m}{3m+2}} + \frac{m(m+1)}{(3m+2)^2}\frac{\tilde{X}^2}{T^2}\right], \\ v(X,t) &= 2\sqrt{gh_0\cos\theta}\frac{m+1}{3m+2}\frac{\tilde{X}}{T}, \end{aligned} \tag{51}$$

where

$$h_0 = \frac{F_0^{1+m/2}}{(g\cos\theta)^{m/2}}, \tilde{X} = \frac{X}{h_0}, T = t\sqrt{\frac{g\cos\theta}{h_0}}.$$

[37] For $m \to \infty$ the solution (51) transforms to the M wave solution obtained by *Savage and Hutter* [1989] and is described by *Pudasaini and Hutter* [2007]. As it follows from (51), its shape in the longitudinal direction is universal for all values m and T. The time evolution of the avalanche shape in the parabolic channel is demonstrated in Figure 9a, it becomes gentle with the lapse of time. The avalanche shape as a function of the channel shape is shown in Figure 9b. This self-similar solution has an evident physical interpretation: landslide particles are "dragged apart" in two directions due to the opposite flows that are strong far from the center. It is interesting to mention that the avalanche height decreases slower in the center than the periphery. The cross-sectional shape of the avalanche influences the speed of the avalanche height, in particular decreasing in extremely narrow channels ($m \to 0$).

[38] Another self-similar solution of (39) and (40) can be obtained by using the self-similar transformation of coordinates

$$\eta = \frac{X}{L(t)}, t = t, \tag{52}$$

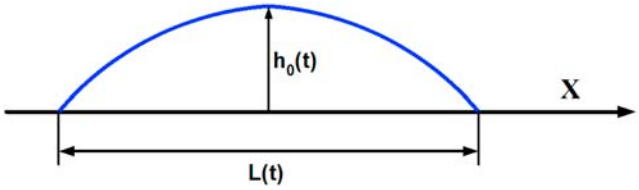

Figure 10. Parabolic cap shape of the avalanche in longitudinal direction.

which transforms equations (39) and (40) to

$$\frac{\partial}{\partial t}\left(h^{\frac{m+1}{m}}\right)+\frac{v-\eta dL/dt}{L}\frac{\partial}{\partial \eta}\left(h^{\frac{m+1}{m}}\right)+\frac{h^{\frac{m+1}{m}}}{L}\frac{\partial v}{\partial \eta}=0 \tag{53}$$

$$\frac{\partial v}{\partial t}+\frac{v-\eta dL/dt}{L}\frac{\partial v}{\partial \eta}+\frac{g\cos\theta}{L}\frac{\partial h}{\partial \eta}=0. \tag{54}$$

[39] Following *Pudasaini and Hutter* [2007] we determine the velocity distribution in the avalanche body as

$$v=\eta\frac{dL}{dt}. \tag{55}$$

[40] After the substitution of (55) in (53) and (54) we obtain two equations with various arguments

$$\frac{\partial}{\partial t}\left(h^{\frac{m+1}{m}}\right)+\frac{dL/dt}{L}h^{\frac{m+1}{m}}=0, \tag{56}$$

$$\frac{\partial h}{\partial \eta}+\frac{\eta L d^2L/dt^2}{g\cos\theta}=0. \tag{57}$$

Both equations are integrated and the corresponding choice of constants can be written as

$$h=h_0(t)\left(1-\eta^2\right), h_0(t)=\frac{L}{2g\cos\theta}\frac{d^2L}{dt^2}, \tag{58}$$

where $L(t)$ is a solution of

$$L^{\frac{2m+1}{m+1}}\frac{d^2L}{dt^2}=q, \tag{59}$$

and q is determined by the initial spreading of the avalanche. So, the avalanche has a parabolic cap shape in the longitudinal direction for any m (Figure 10), but its height and length depend on the cross section of the inclined channel. For a plate, the parabolic cap solution was obtained by *Savage and Hutter* [1989] and is reproduced by *Pudasaini and Hutter* [2007] and its time evolution is quantitatively investigated.

[41] In general, equation (59) is integrated once

$$\left(\frac{dL}{dt}\right)^2=\frac{2q}{L_0^{\frac{m}{m+1}}}\frac{m+1}{m}\left[1-\left(\frac{L_0}{L}\right)^{\frac{m}{m+1}}\right], \tag{60}$$

here we used the initial condition $L(t=0)=L_0$. In the variables

$$l=\frac{L}{L_0}, \tau=t\sqrt{\frac{2q(m+1)}{mL_0^{\frac{3m+2}{m+1}}}}. \tag{61}$$

Equation (60) is presented in the simplified form

$$\tau=\int_1^l\frac{dx}{\sqrt{1-x^{-\frac{m}{m+1}}}}. \tag{62}$$

[42] For each value of m (i.e., specific cross-sectional shapes of the valley) the integral (62) can be evaluated. For $m=\infty$ (inclined plate) it is computed by *Savage and Hutter* [1989] and reproduced by *Pudasaini and Hutter* [2007]. For channels of triangular and parabolic cross section (62) is also calculated explicitly

$$\tau=\left(l+\frac{3}{2}\sqrt{l}\right)\sqrt{1-\frac{1}{\sqrt{l}}}+\frac{3}{4}\log\left[2\left(\sqrt{1-\frac{1}{\sqrt{l}}}+1\right)\sqrt{l}-1\right],$$
$$(m=1)$$
$$\tau=\left(l-l^{1/3}\right)\sqrt{1-l^{-2/3}}, (m=2) \tag{63}$$

The length of the parabolic cap varies in time depending on the shape of the cross section; see Figure 11 (in dimensionless variables).

[43] For large times the avalanche length varies almost linearly in time

$$l(\tau)\approx\tau-\frac{1+m}{2}\tau^{\frac{1}{1+m}}. \tag{64}$$

This leads to the following large-time asymptotic form for the avalanche height

$$h(t)\sim L^{-\frac{m}{m+1}}\sim t^{-\frac{m}{m+1}}. \tag{65}$$

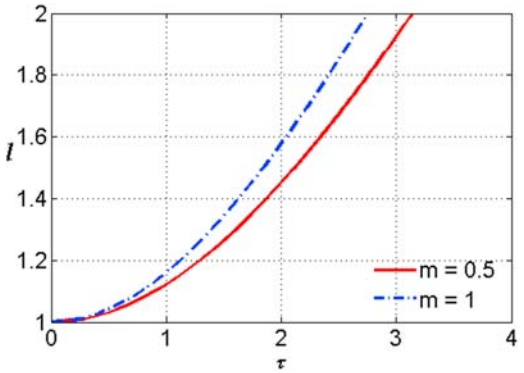

Figure 11. Time evolution of the length of the parabolic cap for various values of m.

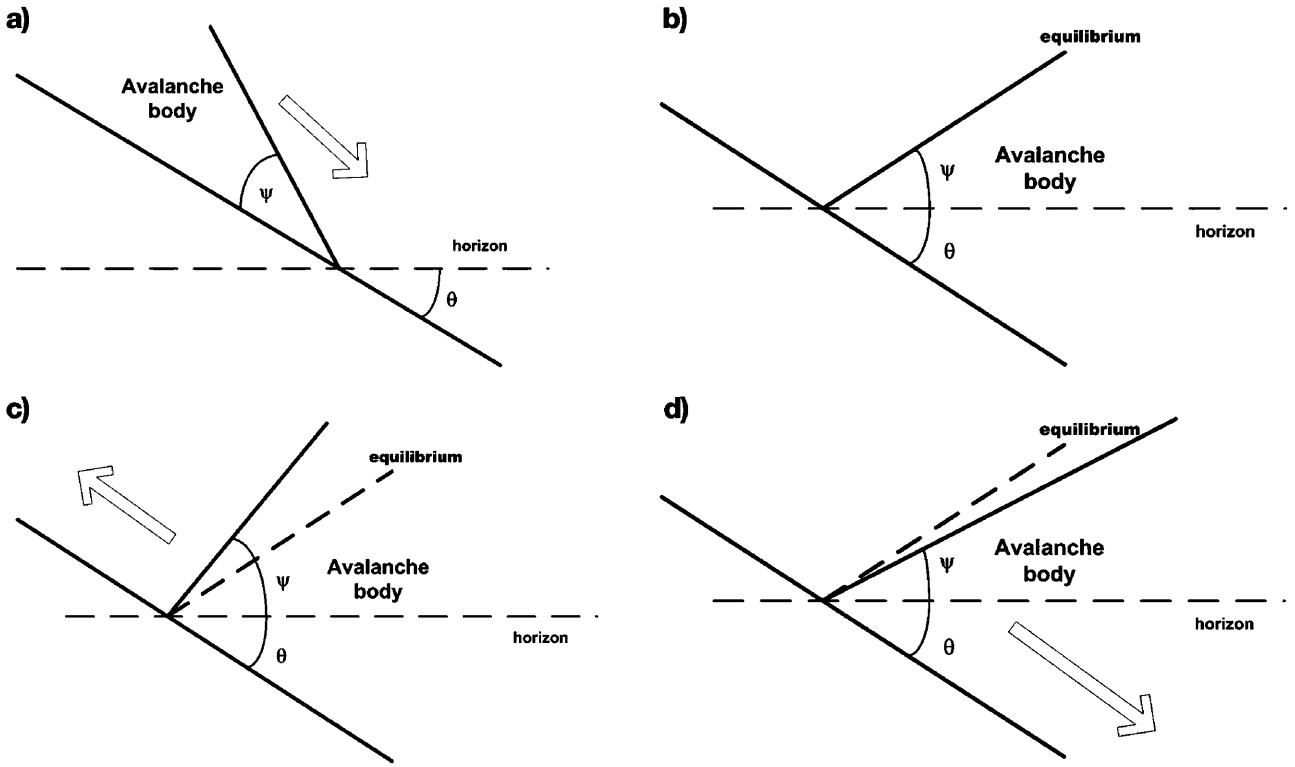

Figure 12. Dynamics of the avalanche with linearly growing height for various surface slopes.

For narrow channels the avalanche height decreases slowly, in particular for channels of parabolic cross section, $L \sim t^{-2/3}$.

[44] Another kind of self-similar solution of the system (5) and (8) can be obtained for the avalanche with linear growing height

$$h(x,t) = \beta[x - x_0(t)],$$
$$u(t) = \frac{dx_0}{dt} = g[\sin\theta - \mu\cos\theta \mathrm{sgn}u - \beta\cos\theta]t, \tag{66}$$

in which β is the slope of the avalanche surface.

[45] The avalanche slides down when $\beta < 0$ ($\Psi = \mathrm{atan}(\beta) > \pi/2$) with constant acceleration that exceeds the sliding component of gravity acceleration reduced by Coulomb friction. In this case the avalanche travels down as a whole (Figure 12a). In the case $\beta > 0$ ($\Psi < \pi/2$) formula (66) describes a rear end of the avalanche. In the frictionless case ($\mu = 0$) the avalanche is nonmoving (static equilibrium) if $\theta = \Psi$ (Figure 12b). If $\theta < \Psi$ the avalanche moves up (Figure 12c) and if $\theta > \Psi$ the avalanche moves down (Figure 12d). When $\mu \neq 0$ the Coulomb friction does not influence the slope of the equilibrium plane. In the vicinity of this equilibrium plane the solution of (66) is sensitive to the friction law (the "jump" function sgn$u$ should replace the smooth function of u) and time evolution is more complicated.

[46] Of course, approximation of an avalanche surface of the constant slope is valid on relatively small distances from the edge, and the solution given here describing the initial dynamics of the real avalanche edge (front or rare) demonstrates that its acceleration differs from the sliding component of the gravity force.

5. Analytical Solutions for Avalanche Dynamics in the Vicinity of its Ends

[47] More general solutions of system (12) can be obtained with the use of the hodograph (Legendre) transformation. Multiplying equation (12) by the Jacobian $\partial(t,x)/\partial(I_+,I_-)$, and assuming that it is not zero (this is discussed later), it can be transformed to

$$\frac{\partial x}{\partial I_\mp} - c_\pm \frac{\partial t}{\partial I_\mp} = 0. \tag{67}$$

System (67) is nonlinear due to the dependence of $c_\pm$ on t, see (13). However, it can be reduced to a linear equation by eliminating x

$$\frac{\partial^2 t}{\partial I_+ \partial I_-} + \frac{3m+2}{2m(I_+ - I_-)}\left(\frac{\partial t}{\partial I_-} - \frac{\partial t}{\partial I_+}\right) = 0. \tag{68}$$

Let us introduce new independent variables:

$$\lambda = \frac{I_+ + I_-}{2} = u - \alpha g t \tag{69}$$

$$\sigma = \frac{I_+ - I_-}{2} = 2\sqrt{\frac{m+1}{m} g h \cos\theta}. \tag{70}$$

Then, equation (68) takes the form

$$\frac{\partial^2 t}{\partial \lambda^2} - \frac{\partial^2 t}{\partial \sigma^2} - \frac{3m+2}{m\sigma}\frac{\partial t}{\partial \sigma} = 0. \tag{71}$$

We should also determine $x(\lambda,\sigma)$. From the system (67), using the new variables (69) and (70), it follows by eliminating t,

$$\alpha g \frac{\partial x}{\partial \sigma} = u\frac{\partial u}{\partial \sigma} + \frac{m\sigma}{2(m+1)} - \frac{m\sigma}{2(m+1)}\frac{\partial u}{\partial \lambda}. \tag{72}$$

This equation can be integrated when the velocity, u, is expressed in terms of the wave function $\Phi(\sigma,\lambda)$

$$u = \frac{1}{\sigma}\frac{\partial \Phi}{\partial \sigma}. \tag{73}$$

An equation for this wave function can be deduced from (71). First, with the use of (69) it transforms to the wave equation for u and second, after the substitution of (73) it can be once integrated over σ

$$\frac{\partial^2 \Phi}{\partial \lambda^2} - \frac{\partial^2 \Phi}{\partial \sigma^2} - \frac{m+2}{m\sigma}\frac{\partial \Phi}{\partial \sigma} = 0. \tag{74}$$

[48] The integration of (72) together with (69), (70) and (73) allows determination of all physical variables, which are given below

$$h = \frac{1}{4g\cos\theta}\frac{m}{m+1}\sigma^2, u = \frac{1}{\sigma}\frac{\partial \Phi}{\partial \sigma} \tag{75}$$

$$\alpha g x = \frac{u^2}{2} + \frac{m\sigma^2}{4(m+1)} - \frac{m}{2(m+1)}\frac{\partial \Phi}{\partial \lambda}, t = \frac{u-\lambda}{g\alpha}. \tag{76}$$

[49] So, the initial set of the nonlinear shallow water equations for gravity driven flow in an inclined channel of parabolic-like cross section is reduced to the linear wave equation (74), and all physical variables can be found via the wave function Φ using simple operations. The main advantage of this form is that the moving (unknown) avalanche edge corresponds now to $\sigma = 0$ (since its height $h = 0$) and, therefore, equation (74) should be solved in the half-space $\sigma \geq 0$ with the fixed boundary. Such a transformation generalizes the original Carrier – Greenspan transformation for water waves above a beach of constant slope [*Carrier and Greenspan*, 1958], and is reduced to it for a plane beach ($m \to \infty$) and zero friction. In fact, it was also derived for inviscid water waves in an inclined channel [*Zahibo et al.*, 2006; *Choi et al.*, 2008], and our approach extends it to the avalanche flow with Coulomb friction. In the cited papers the wave shoaling, reflection and run-up were analyzed, however, for avalanche dynamics "non-wave" solutions are more important.

[50] This approach is used below to study the evolution of a landslide initially at rest ($u = 0$). According to the right equation (76) the initial conditions should be formulated at $\lambda = 0$. They follow from (73) and the left equation (76); thus,

$$\Phi(\sigma, \lambda = 0) = 0 \tag{77}$$

$$\left.\frac{\partial \Phi}{\partial \lambda}\right|_{\lambda=0} = \frac{\sigma^2}{2} - \frac{2(m+1)\alpha g}{m}x(\sigma), \tag{78}$$

where $x(\sigma)$ is found from the initial landslide shape in the longitudinal direction, $h(x) = \frac{1}{4g\cos\theta}\frac{m}{m+1}\sigma^2$, see (75).

[51] The boundary condition on the avalanche edge ($\sigma = 0$) is the boundedness of the physical variables, and therefore, the wave function, $\Phi(0,\lambda)$. In general, another boundary ($h = h_{\max}$ or $\sigma = \sigma_{\max}$) is not fixed, and it should be determined from the solution. It is fixed only if: i) the initial avalanche height tends to a constant (as in the dam break problem); and ii) the avalanche height grows monotonically with the distance from the edge. For simplicity the last variant is analyzed here and we solve the wave equation (74) in the domain $0 \leq \sigma < \infty$. In this case the boundary condition for $\sigma \to \infty$ is the Sommerfeld radiation condition (no disturbances come from infinity).

[52] The solution of the Cauchy problem for the wave equation (74) for the semiaxis is well known [*Courant and Hilbert*, 1953], and in general it can be expressed through Bessel functions. It is simplified for the parabolic cross section of the channel ($m = 2$). For case $m = 2$, the wave equation (74), after the substitution

$$\Phi(\sigma, \lambda) = \frac{\Psi(\sigma, \lambda)}{\sigma}, \tag{79}$$

transforms to the constant-coefficient wave equation

$$\frac{\partial^2 \Psi}{\partial \lambda^2} - \frac{\partial^2 \Psi}{\partial \sigma^2} = 0, \tag{80}$$

which should be solved for $\sigma \geq 0$. Its solution is

$$\Psi(\sigma, \lambda) = \begin{cases} \Omega(\sigma+\lambda) - \Omega(\lambda-\sigma) & 0 < \sigma < \lambda, \\ \Omega(\sigma+\lambda) - \Omega(\sigma-\lambda) & \lambda < \sigma, \end{cases} \tag{81}$$

and satisfies the initial condition (77), reduced to $\Psi(\sigma,0) = 0$, and the boundary condition of the bounded quantity of $\Phi(\lambda, \sigma = 0)$ reduced to $\Psi(0,\lambda) = 0$.

[53] The function $\Omega(\xi \geq 0)$ is found from the initial avalanche shape (78) that, after substitution of (81), transforms into the ODE

$$\frac{2}{\sigma}\frac{d\Omega(\sigma)}{d\sigma} = \frac{\sigma^2}{2} - 3\alpha g x(\sigma), h(x) = \frac{1}{6g\cos\theta}\sigma^2. \tag{82}$$

Below the dimensionless form of these equations is applied. Dimensionless variables are

$$\sigma'|\lambda' = \frac{\sigma|\lambda}{\sqrt{gh_0}}, \Phi' = \frac{\Phi}{(gh_0)^{3/2}}, H = \frac{h\cos\theta}{h_0}, \\ V = \frac{u}{\sqrt{gh_0}}, X = \frac{\alpha}{h_0}x, T = \alpha t\sqrt{\frac{g}{h_0}}, \tag{83}$$

where h_0 is the characteristic avalanche height. We keep X and T as nondimensional variables of the spatial coordinate and time and introduce $X' = X - T^2/2$ for the accelerated reference system. Parameters of the hodograph transformation are rewritten in the final form (primes are omitted)

$$H = \frac{\sigma^2}{6}, X = \frac{V^2}{2} + \frac{\sigma^2}{6} - \frac{1}{3}\frac{\partial \Phi}{\partial \lambda},$$
$$T = V - \lambda, \frac{2}{\sigma}\frac{d\Omega(\sigma)}{d\sigma} = \frac{\sigma^2}{2} - 3X(\sigma, 0). \tag{84}$$

[54] Let us consider the dynamics of the avalanche front when its initial shape in the longitudinal direction is described by

$$X(T=0) = -q\sigma^{\gamma} = -q(6H)^{\gamma/2}, q > 0. \tag{85}$$

Substitution of (85) into the last expression in (84) after integrating leads to the explicit definition of the function $\Omega(\sigma)$ as follows:

$$\Omega(\sigma) = \frac{\sigma^4}{16} + \frac{3q}{2(\gamma+2)}\sigma^{\gamma+2}, \tag{86}$$

and, therefore, using (79) and (81) the function $\Phi(\sigma,\lambda)$ is determined for all values of its arguments.

[55] As a first example, an avalanche with linearly growing height ($\gamma = 2$) is analyzed; this front is curvature free. In this case (the details of calculations are given in Appendix A)

$$\Phi(\lambda, \sigma) = \frac{1+6q}{2}\left(\sigma^2\lambda + \lambda^3\right), \tag{87}$$

Which, with the use of (84), leads to an explicit formula for the avalanche height as a function of time,

$$H(X,T) = \frac{1}{6q}\left(\frac{VT}{2} - X\right), V(T) = \frac{(1+6q)}{6q}T. \tag{88}$$

This solution coincides with the self-similar solution (66) obtained directly from the basic equations. The avalanche shape in the longitudinal direction does not change in time, and it falls off with constant acceleration depending on the avalanche slope.

[56] Another example is an avalanche with the square root singularity on its front ($\gamma = 4$, $H \sim X^{1/2}$). As the curvature of the avalanche surface in the frontal zone is positive ($d^2H/dx^2 > 0$) the function is concave. In this case (we will not give here details of the calculations which are similar to those given in Appendix A)

$$\Omega(\sigma) = \frac{\sigma^4}{16} + \frac{q}{4}\sigma^6, \tag{89}$$

and the function $\Phi(\sigma,\lambda)$ is fully determined for $\sigma \geq 0$

$$\Phi = \frac{1}{2}\left(\sigma^2\lambda + \lambda^3\right) + q\left(3\sigma^4\lambda + 10\sigma^2\lambda^3 + 3\lambda^5\right). \tag{90}$$

As a result, the parametric equations for the avalanche characteristics can be found

$$T = q\left(12\sigma^2\lambda + 20\lambda^3\right),$$
$$X = q\left(2\sigma^2\lambda^2 + 15\lambda^4 - \sigma^4\right) + \frac{T^2}{2}, V = \lambda + T. \tag{91}$$

[57] At small times and far from the front ($\lambda \sim T/12q\sigma^2$) the avalanche shape is described by the explicit asymptotic expression followed from (91)

$$X(H,T) \approx -36qH^2 + \left(1 + \frac{1}{216qH}\right)\frac{T^2}{2}, \tag{92}$$

which is valid far from the front edge

$$H \gg \left[\frac{1}{q72\sqrt{18/5}}\right]^{2/3} T^{2/3}. \tag{93}$$

So, the main part of the avalanche begins to move with an acceleration equal in absolute value to 1 (the projection of the gravity acceleration reduced by Coulomb friction in dimensional system is $g\alpha$), in the zone of large heights. The part of the avalanche with moderate heights falls with larger acceleration, and its value grows with decreasing height. Near the front edge where the height satisfies equation (93) with the opposite inequality sign, the asymptotic expression followed from (91) is valid

$$X(H,T) \approx -36qH^2 + \frac{3}{4\sqrt[3]{20q}}T^{4/3} + \frac{T^2}{2}, \tag{94}$$

and this part moves with variable acceleration. Therefore, the front part of the avalanche is stretched in time. These conclusions, made on the basis of the asymptotic analysis, are confirmed by direct calculations of equation (91); see Figure 13 where the avalanche shape is drawn in dimensionless accelerated reference coordinates X'.

[58] The front moves quickly, and the avalanche shape tends to the equilibrium state (63) that corresponds to the avalanche with the linearly growing height. The distance covered by the avalanche front is described by the curve

$$X(T) = \frac{3}{4\sqrt[3]{20q}}T^{4/3} + \frac{T^2}{2}, \tag{95}$$

following from (91) at $\sigma = 0$. At large times the front also moves with acceleration 1 ($g\alpha$ in the dimensional system), whereas the main avalanche body confirms its tendency to the equilibrium state.

[59] The avalanche contour in time is displayed in Figure 14 for different times. It is evident that the avalanche contour on the X'-Y plane tends from almost strait line for small X' to the "tongue" shape with time.

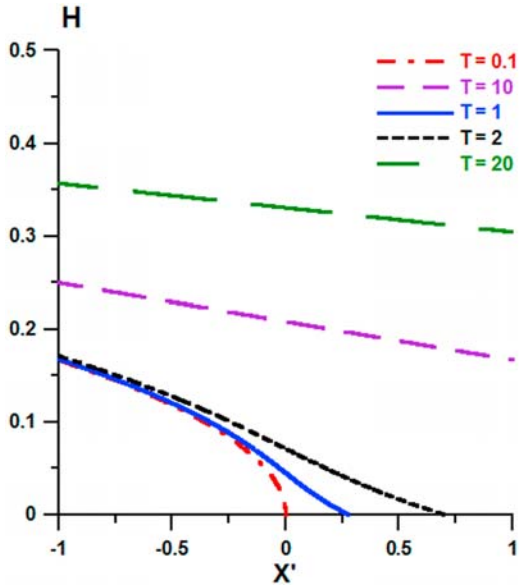

Figure 13. Time evolution of the frontal zone of avalanche for $q = 1$ (initial shape is $H \sim X^{0.5}$).

[60] The third example is an avalanche whose initial shape is described by equation (85) with $\gamma = 1$ when the avalanche height grows as X^2 with distance from the edge (a beak-shaped front). As the curvature of this front is negative, the wave function is found in the form (mathematical details are the same as given in Appendix A)

$$\Phi(\sigma,\lambda) = \begin{cases} \frac{\lambda}{2}(\sigma^2+\lambda^2) + q(\sigma^2+3\lambda^2) & \sigma < \lambda \\ \frac{\lambda}{2}(\sigma^2+\lambda^2) + q\frac{\lambda}{\sigma}(3\sigma^2+\lambda^2) & \sigma > \lambda. \end{cases} \quad (96)$$

Consequently, the parametric expressions for the avalanche shape can be obtained: for $\sigma < \lambda$ we obtain

$$X(\sigma,\lambda) = 2q\lambda - 4q^2, T(\sigma,\lambda) = 2q, \quad (97)$$

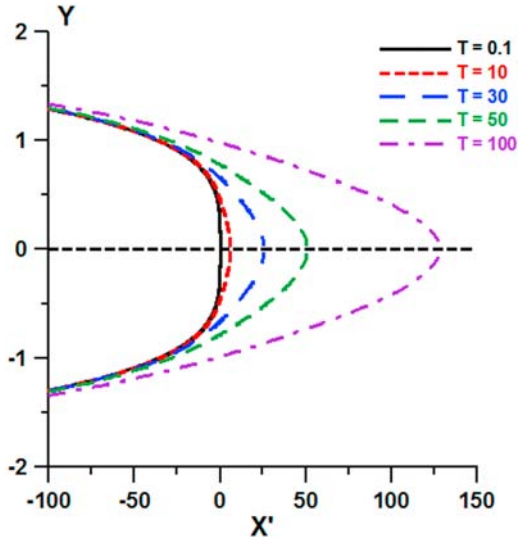

Figure 14. Spatial structure of the avalanche for times $T =$ 10, 30, 50, 100 (initial shape is $H \sim X^{0.5}$).

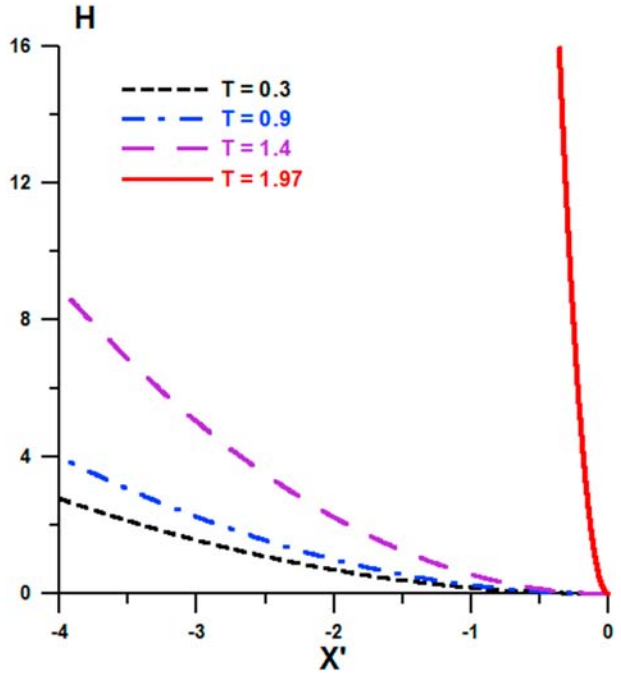

Figure 15. Initially parabolic avalanche profiles for various times before shock formation ($q = 1$, $H \sim X^2$).

while for $\sigma > \lambda$ we deduce

$$X(\sigma,\lambda) = q\frac{\lambda^2}{\sigma}\left(2-\frac{\lambda^2}{\sigma^2}\right) - q\sigma + \frac{q^2\lambda^2}{2\sigma^2}\left(3-\frac{\lambda^2}{\sigma^2}\right)^2,$$
$$T(\sigma,\lambda) = \frac{q\lambda}{\sigma}\left(3-\frac{\lambda^2}{\sigma^2}\right). \quad (98)$$

On the avalanche front, expression (95) becomes inconsistent. The Jacobian of the hodograph transformation vanishes there which leads to the appearance of multivalued functions. Physically, this means that a shock is formed on the avalanche front. Far from the edge and at small times the avalanche shape in the longitudinal direction is described by the asymptotic expression

$$H(X,T) \approx \chi(T)[X - X_0(T)]^2,$$
$$X_0(T) = \frac{T^2}{2}, \chi(T) = \frac{1}{6q^2}\left(1+\frac{2T^2}{9q^2}\right). \quad (99)$$

[61] The avalanche falls under the action of gravity acceleration (1 in the dimensionless system), and its slope increases with time. In finite time the steepness of the flow increases for each point on the avalanche which causes breaking. The breaking time, estimated from the exact formula (97), for $\lambda \sim \sigma$ corresponds to $T_{br} \sim 2q$. The avalanche shape for various instances is shown in Figure 15 for $q = 1$. The evident tendency to shock formation for the time close to $2q$ is observed. It is necessary to note that the avalanche shape is close to a parabolic curve, $H \sim X^2$ everywhere, not only in the asymptotic case predicted by (99).

[62] To consider the further evolution of the avalanche with the beak-shaped front it is necessary to take into account the real configuration of the flow shape at large

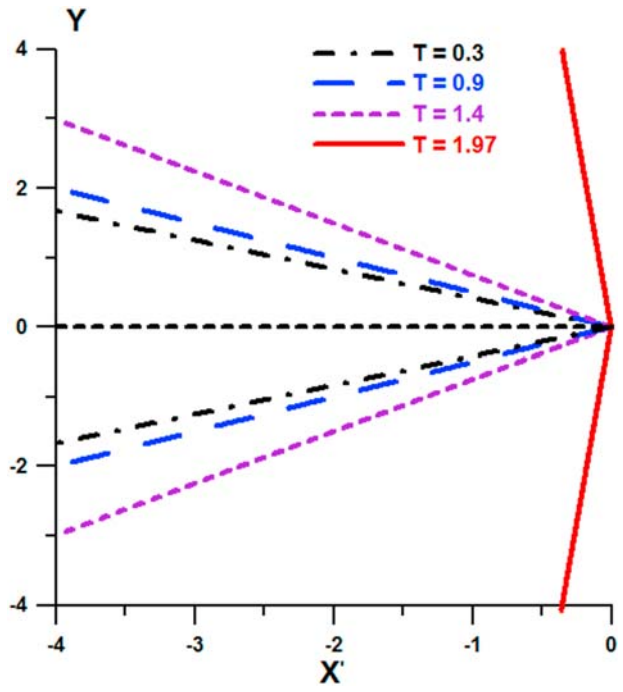

Figure 16. Spatial structure of the initially parabolic avalanche for various times.

heights which is expected far from the parabola. Anyhow the beak-shaped front should break. The avalanche contours in time for this case are presented in Figure 16. In this case the avalanche contour on X'-Y plane tends from a triangular shape for small T to almost a straight line for T tending to 2.

[63] Thus, tendencies of the evolution of the avalanche front depend on the curvature. Flows with positive curvature in the front spread in time, their fronts become gentle, and their curvatures tend to zero. The curvature increases and breaks for the avalanche with a negative curvature in the front. The equilibrium shape has no curvature on its front and moves as a whole.

[64] The same approach can be applied to study the behavior of the rear end of an avalanche (for simplicity we assume here $\mu = 0$). For an avalanche with linearly growing height ($\gamma = 2$) on the rear end, the solution can be obtained from (88) by changing the sign of q. There are three different kinds of solutions that correspond to various values of q. When $q = -1/6$, the avalanche surface represents a horizontal plane (inclined by the Coulomb friction), and there is no movement. When $q < -1/6$, the rear end of the avalanche is inclined down, and it falls down as a whole with constant acceleration. When $q > -1/6$ the rear end is inclined up and moves upward. As mentioned above, this solution coincides with the self-similar solution (63) obtained directly from the basic equations.

[65] For an avalanche with the square root singularity on the rear end ($\gamma = 4$, $H \sim X^{1/2}$) the design formula is (91) where $q < 0$. New features of avalanche dynamics follow from the approximate equation (92) for small times as the coefficient changes its sign (that represents the acceleration). The zone of big avalanche heights $H > H_{cr} = \frac{1}{216q}$ should move down, whereas a rear end of avalanche should move up. This difference can be understood if we compare the shapes of avalanches with linear and square root dependences on height. On the rear end, the avalanche with square root singularity has high steepness like the avalanche with the linearly growing height inclined down to horizon. As shown, such avalanches move up. The periphery of the avalanche has small steepness and the avalanche surface is inclined down (i.e., below the horizon); such avalanches move down. In Figure 17 the curves $X(T)$ for various points on the rear slope computed from (91) for $q = -1$ are shown. The behavior of the curves corresponds to what was predicted in the framework of the perturbation theory based on equation (92). At small times the avalanche rear part moves up, though at large times the avalanche falls down as a whole. All curves diverge in time, and therefore, the avalanche shape remains smooth.

[66] For the trajectory of the rear point of the avalanche ($\sigma = 0$) a simple analytical formula can be given

$$X(T) = -\frac{3}{4\sqrt[3]{20|q|}}T^{4/3} + \frac{T^2}{2}, \qquad (100)$$

to compare with (95). This curve is plotted in Figure 18 for $q = -1$. The rear end of the avalanche moves up until $T^* = (20|q|)^{-1/2}$, and then it falls. The maximum height of avalanche in the upward motion is

$$|X|^* = 1/80|q|. \qquad (101)$$

[67] The evolution of the rear end with the initial square root singularity in the usual coordinate system is shown in Figure 19a for $q = -1$. It is demonstrated that these points move up and then fall, which confirms our asymptotic analysis. Only the main body of the avalanche falls. The shape of the varied rear end becomes more linear in time. This is clearly seen in Figure 19b where the avalanche shape is shown in the accelerated reference system, and in this case the avalanche moves to the left. So, the rear end of the avalanche has the tendency to become linear. The given examples show the applicability of the hodograph transformation to describe analytically the various scenarios of avalanche dynamics in inclined channels of parabolic-like

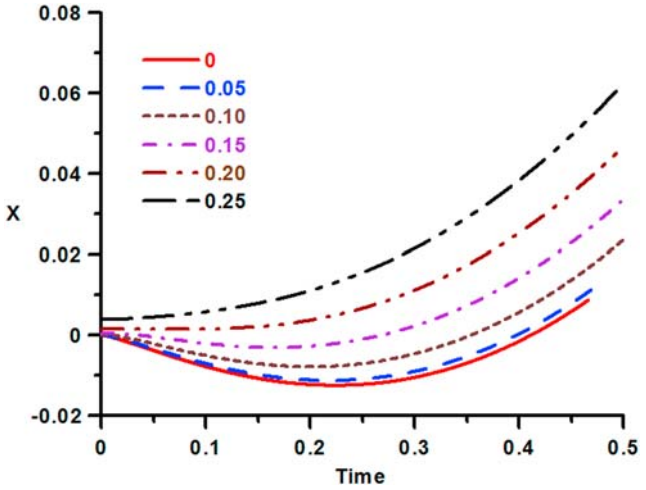

Figure 17. Curves $X(T)$ for various points of rear slope (numbers indicate values of σ).

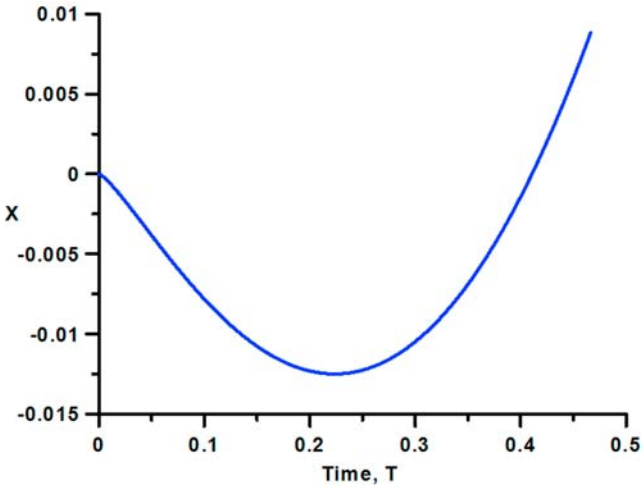

Figure 18. Trajectory of the rear end of avalanche for $q = 1$ (initial shape is $H \sim X^{0.5}$).

shape. In comparison with the self-similar solutions that describe the nonbreaking dynamics of the avalanche initially at rest (section 4), new solutions demonstrate that, depending on the initial shape, the avalanche can move with a smooth shape as well as with a shock front. The formation of shock fronts in landslides and two-phase granular flows has been pointed out in numerical experiments performed by *Fine et al.* [2003] and *Pelanti et al.* [2008].

6. Conclusion

[68] Computing avalanche dynamics is an extremely important task in natural hazard assessments, and various physical and numerical models are developed. The analytical solutions allow studying the physical features of such processes (the beginning of movement, the direction of the avalanche motion, spreading, forming of shocks and so on). Several analytical solutions for avalanche dynamics in mountain valleys approximated by narrow channels (sometimes, granular flows in wide channels can be propagated as self-channeling narrow flows, and this effect has been reproduced recently numerically by *Mangeney et al.* [2007a]) of parabolic-like cross section are obtained here in the framework of the simplified version of the Savage-Hutter model. Some of them generalize known solutions for avalanche propagation along the inclined plate (the dam break problem, the parabolic cap, the M wave, the Riemann wave). The quality of avalanche dynamics in the longitudinal direction is similar to that of avalanches along channels of arbitrary cross section. However, the spatial structure of the avalanche is different in channels of different cross sections. Quantitative characteristics of avalanche dynamics depend on the cross-sectional shape and, in narrow channels, for instance, nonlinear processes develop more intensively for the same avalanche heights.

[69] In the present paper a new approach to investigate avalanche dynamics is suggested. It is based on the hodograph (Legendre) transformation and can be applied for avalanches of different initial shapes. The derived solutions show that the linear avalanche shape is the equilibrium shape which moves along the mountain flank without changing its shape (it also follows from the direct self-similar solution). Avalanche frontal shapes that may be approximated by the equation with power dependence on the coordinate $h \sim x^a$ on the front, have a tendency to break if the power a is more than one and a tendency to form the frontal "tongue" if the power a is less than one. Furthermore, the rear end of the avalanche is studied and the possibility of nonmonotonic motion of the rear end is found. All the solutions obtained above describe avalanche dynamics above solid basalt. In fact, an erodible bed can increase the mobility of the avalanche which can propagate in the form of traveling waves; this interesting geophysical phenomenon is in the process of being analyzed [*Mangeney et al.*, 2007b; *Lucas and Mangeney*, 2007].

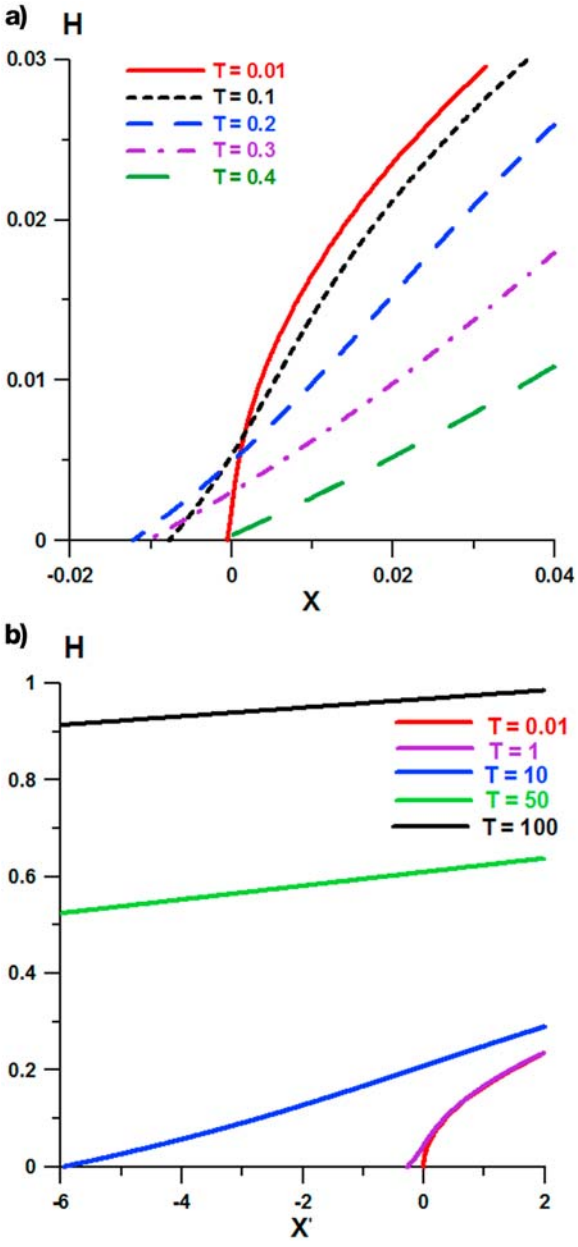

Figure 19. Evolution of the rear end of avalanche for $q = 1$ (initial shape is $H \sim X^{0.5}$) (a) in the usual coordinate system and (b) in the accelerated reference system.

[70] In fact, the simplified frictional rheology (constant friction angle) is used to obtain analytical solutions. As pointed by *Pirulli and Mangeney* [2008], various rheological models can be applied to model avalanche dynamics but only the frictional rheology has allowed the back analysis of the historical events of the rock avalanches: Frank (Canada, 1903) and Val Pola (Italy, 1987). The main advantage of this simplified model is that only one parameter (the friction angle) has to be calibrated. In the case of the inclined channel the second parameter (the shape factor) should be taken into account and it can be determined for real mountain valleys. This is very important for the prediction of potential events, and the analytical solutions described above allow estimating possible scenarios taking into account the lack of data of the potential events. The simple analytical solutions presented here may be very useful to analyze and recover scaling laws observed in laboratory experiments of natural landslides [e.g., *Mangeney-Castelnau et al.*, 2005; *Lucas and Mangeney*, 2007]. They can be also used to test numerical codes of avalanche dynamics in the valleys of complicated geometry.

Appendix A

[71] Let us consider avalanche dynamics with linear growing height in the front ($\gamma = 2$). In this case equation (86) yields

$$\Omega(\sigma) = \frac{1+6q}{16}\sigma^4. \tag{A1}$$

[72] Substituting (A1) into (81) we may compute the function Ψ

$$\Psi(\sigma,\lambda) = \frac{1+6q}{2}\sigma\lambda\left(\sigma^2+\lambda^2\right), \tag{A2}$$

and then the wave function (79)

$$\Phi(\sigma,\lambda) = \frac{1+6q}{2}\lambda\left(\sigma^2+\lambda^2\right). \tag{A3}$$

Now we may calculate all physical variables. In particular, the velocity is given by

$$V = \frac{1}{\sigma}\frac{\partial\Phi}{\partial\sigma} = (1+6q)\lambda. \tag{A4}$$

The third equation in (84) determines the time

$$T = V - \lambda = 6q\lambda. \tag{A5}$$

As a result, arguments λ and σ can be expressed explicitly through physical variables T and H (as the first equation in (84) determines the relation between H and σ). Finally, the velocity is a function of time only

$$V = \frac{1+6q}{6q}T, \tag{A6}$$

and X is computed from the second equation (84)

$$X = \frac{1+6q}{12q}T^2 - 6qH, \tag{A7}$$

or

$$H = \frac{1}{6q}\left(\frac{VT}{2} - X\right), \tag{A8}$$

see (88). In other cases of the initial distribution of the avalanche height in the longitudinal direction, formulas for physical variables are implicit and the computer is required to perform algebraic manipulations.

[73] **Acknowledgments.** Partial support from the grants CPER (2007–2013), ANR project (Vitesss), ARC (DP0988449), RFBR (08-05-00069, 08-05-91850, 09-05-91222, 09-05-00204) is gratefully acknowledged. We thank Kolumban Hutter and another anonymous reviewer for their detailed comments that helped to improve this paper.

References

Assier-Rzadkiewicz, S., P. Heinrich, P. C. Sabatier, B. Savoyer, and J. F. Bourillet (2000), Numerical modeling of a landslide-generated tsunami: The 1979 Nice event, *Pure Appl. Geophys.*, *157*, 1707–1727, doi:10.1007/PL00001057.

Bouchut, F., and M. Westdickenberg (2004), Gravity driven shallow water models for arbitrary topography, *Commun. Math. Sci.*, *2*, 359–389.

Bouchut, F., A. Mangeney-Castelnau, B. Perthame, and J.-P. Vilotte (2003), A new model of Saint Venant and Savage-Hutter type for gravity driven shallow water flows, *C. R. Acad. Sci., Ser. I*, *336*, 531–536.

Bouchut, F., E. D. Fernandez-Nieto, A. Mangeney, and P.-Y. Lagree (2008), On new erosion models of Savage-Hutter type for avalanches, *Acta Mech.*, *199*, 181–208, doi:10.1007/s00707-007-0534-9.

Carrier, G. F., and H. P. Greenspan (1958), Water waves of finite amplitude on a sloping beach, *J. Fluid Mech.*, *4*, 97–109, doi:10.1017/S0022112058000331.

Choi, B. H., E. Pelinovsky, D. C. Kim, I. Didenkulova, and S. B. Woo (2008), Two- and three-dimensional computation of solitary wave run-up on non-plane beach, *Nonlinear Process. Geophys.*, *15*(3), 489–502.

Courant, R., and D. Hilbert (1953), *Methods of Mathematical Physics*, 561 pp., John Wiley, New York.

Fernandez-Feria, R. (2006), Dam-break flow for arbitrary slopes of the bottom, *J. Eng. Math.*, *54*, 319–331, doi:10.1007/s10665-006-9034-5.

Fernandez-Nieto, E. D., F. Bouchut, D. Bresch, M. J. Castro Diaz, and A. Mangeney (2008), A new Savage-Hutter type model for submarine avalanches and generated tsunami, *J. Comput. Phys.*, *227*, 7720–7754, doi:10.1016/j.jcp.2008.04.039.

Fine, I. V., A. B. Rabinovich, R. E. Thomson, and E. A. Kulikov (2003), Numerical modeling of tsunami generation by submarine and subaerial landslides, in *Submarine Landslides and Tsunamis*, vol. 21, *Earth and Environmental Sciences*, *NATO Sci. Ser.*, vol. 4, edited by A. Yalçiner et al., pp. 69–88, Kluwer, Boston.

Fine, I. V., A. B. Rabinovich, B. D. Bornhold, R. E. Thomson, and E. A. Kulikov (2005), The Grand Banks landslide-generated tsunami of November 18, 1929: Preliminary analysis and numerical modeling, *Mar. Geol.*, *215*, 45–57, doi:10.1016/j.margeo.2004.11.007.

Gray, J. M. N. T., M. Wieland, and K. Hutter (1999), Gravity-driven free surface flow of granular avalanches over complex basal topography, *Proc. R. Soc. London, Ser. A*, *455*, 1841–1874, doi:10.1098/rspa.1999.0383.

Heinrich, P., A. Mangeney, S. Guibourg, R. Roche, G. Boudon, and J. Cheminée (1998), Simulation of water waves generated by a potential debris avalanche in Montserrat, Lesser Antilles, *Geophys. Res. Lett.*, *25*(19), 3697–3700, doi:10.1029/98GL01407.

Heinrich, P., S. Guibourg, A. Mangeney, and R. Roche (1999), Numerical modeling of a landslide-generated tsunami following a potential explosion of the Montserrat volcano, *Phys. Chem. Earth*, *24*(2), 163–168, doi:10.1016/S1464-1895(99)00013-7.

Heinrich, P., G. Boudon, J. C. Komorowski, R. S. J. Sparks, R. Herd, and B. Voight (2001), Numerical simulation of the December 1997 debris avalanche in Montserrat, Lesser Antilles, *Geophys. Res. Lett.*, *28*(13), 2529–2532, doi:10.1029/2001GL012968.

Imamura, F., and E. C. Gica (1996), Numerical model for tsunami generation due to subaqueous landslide along a coast, *Sci. Tsunami Hazards*, *14*(1), 13–28.

Kerswell, R. R. (2005), Dam break with the Coulomb friction: A model for granular slumping?, *Phys. Fluids*, *17*, 057101, doi:10.1063/1.1870592.

Le Friant, A., P. Heinrich, C. Deplus, and G. Boudon (2003), Numerical simulation of the last flank-collapse event of Montagne Pelée, Martinique, Lesser Antilles, *Geophys. Res. Lett.*, *30*(2), 1034, doi:10.1029/2002GL015903.

Le Friant, A., G. Boudon, J.-C. Komorowski, P. Heinrich, and M. P. Semet (2006), Potential flank-collapse of Soufriere Volcano, Guadeloupe, Lesser Antilles? Numerical simulation and hazards, *Nat. Hazards*, *39*, 381–393, doi:10.1007/s11069-005-6128-8.

Liu, P. L.-F., P. Lynett, and C. E. Synolakis (2003), Analytical solutions for forced long waves on a sloping beach, *J. Fluid Mech.*, *478*, 101–109, doi:10.1017/S0022112002003385.

Luca, I., K. Hutter, Y. C. Tai, and C. Y. Kuo (2009), A hierarchy of avalanche models on arbitrary topography, *Acta Mech.*, *205*, 121–149, doi:10.1007/s00707-009-0165-4.

Lucas, A., and A. Mangeney (2007), Mobility and topographic effects for large Valles Marineris landslides on Mars, *Geophys. Res. Lett.*, *34*, L10201, doi:10.1029/2007GL029835.

Mangeney, A., P. H. Heinrich, R. Roche, G. Boudon, and J. L. Cheminee (2000a), Modeling of debris avalanche and generated water waves: Application to real and potential events in Montserrat, *Phys. Chem. Earth*, *25*(9–11), 741–745, doi:10.1016/S1464-1895(00)00115-0.

Mangeney, A., P. Heinrich, and R. Roche (2000b), Analytical solution for testing debris avalanche numerical models, *Pure Appl. Geophys.*, *157*, 1081–1096, doi:10.1007/s000240050018.

Mangeney, A., F. Bouchut, N. Thomas, J. P. Vilotte, and M. O. Bristeau (2007a), Numerical modeling of self-channeling granular flows and of their levee-channel deposits, *J. Geophys. Res.*, *112*, F02017, doi:10.1029/2006JF000469.

Mangeney, A., L. S. Tsimring, D. Volfson, I. S. Aranson, and F. Bouchut (2007b), Avalanche mobility induced by the presence of an erodible bed and associated entrainment, *Geophys. Res. Lett.*, *34*, L22401, doi:10.1029/2007GL031348.

Mangeney-Castelnau, A., J.-P. Vilotte, M. O. Bristeau, B. Perthame, F. Bouchut, C. Simeoni, and S. Yerneni (2003), Numerical modeling of avalanches based on Saint Venant equations using a kinetic scheme, *J. Geophys. Res.*, *108*(B11), 2527, doi:10.1029/2002JB002024.

Mangeney-Castelnau, A., F. Bouchut, J. P. Vilotte, E. Lajeunesse, A. Aubertin, and M. Pirulli (2005), On the use of Saint Venant equations to simulate the spreading of a granular mass, *J. Geophys. Res.*, *110*, B09103, doi:10.1029/2004JB003161.

Miller, D. J. (1960), Alaska Earthquake on July 10, 1958: Giant wave in Lituya Bay, *Bull. Seismol. Soc. Am.*, *50*(2), 253–266.

Pelanti, M., F. Bouchut, and A. Mangeney (2008), A Roe-type scheme for two-phase shallow granular flows over variable topography, *Math. Modell. Numer. Anal.*, *42*, 851–885, doi:10.1051/m2an:2008029.

Pelinovsky, E. (2003), Analytical models of tsunami generation by submarine landslides, in *Submarine Landslides and Tsunamis*, vol. 21, *Earth and Environmental Sciences*, *NATO Sci. Ser.*, vol. 4, edited by A. Yalçiner et al., pp. 111–128, Kluwer, Boston.

Pelinovsky, E., and A. Poplavsky (1996), Simplified model of tsunami generation by submarine landslides, *Phys. Chem. Earth*, *21*(12), 13–17, doi:10.1016/S0079-1946(97)00003-7.

Pelinovsky, E. N., and E. N. Troshina (1994), Propagation of long waves in straits, *Phys. Oceanogr.*, *5*(1), 43–48, doi:10.1007/BF02197568.

Pelinovsky, E., N. Zahibo, P. Dunkley, M. Edmonds, R. Herd, T. Talipova, A. Kozelkov, and I. Nikolkina (2004), Tsunami generated by the volcano eruption on July 12–13 2003 at Montserrat, Lesser Antilles, *Sci. Tsunami Hazards*, *22*(1), 44–57.

Pirulli, M., and A. Mangeney (2008), Results of back-analysis of the propagation of rock avalanches as a function of the assumed rheology, *Rock Mech. Rock Eng.*, *41*(1), 59–84, doi:10.1007/s00603-007-0143-x.

Pudasaini, S. P., and K. Hutter (2007), *Avalanche Dynamics: Dynamics of Rapid Flows of Dense Granular Avalanches*, 602 pp., Springer, New York.

Rudenko, O. V., A. L. Sobisevich, and L. E. Sobisevich (2007), Nonlinear dynamics of slope flows: Simple models and exact solutions, *Dokl. Earth Sci.*, *416*(1), 1109–1113, doi:10.1134/S1028334X07070288.

Sammarco, P., and E. Renzi (2008), Landslide tsunamis propagating along a plane beach, *J. Fluid Mech.*, *598*, 107–119, doi:10.1017/S0022112007009731.

Savage, S. B., and K. Hutter (1989), The motion of a finite mass of granular material down a rough incline, *J. Fluid Mech.*, *199*, 177–215, doi:10.1017/S0022112089000340.

Savage, S. B., and K. Hutter (1991), Dynamics of avalanches of granular materials from initiation to run-out. Part 1: Analysis, *Acta Mech.*, *86*, 201–223, doi:10.1007/BF01175958.

Stoker, J. J. (1957), *Water Waves: The Mathematical Theory with Applications*, Interscience, New York.

Tinti, S., E. Bortolucci, and C. Chlavettieri (2001), Tsunami excitation by submarine slides in shallow-water approximation, *Pure Appl. Geophys.*, *158*, 759–797, doi:10.1007/PL00001203.

Voight, B., J.-C. Komorowski, G. Norton, A. Belousov, M. Belousova, G. Boudon, P. W. Francis, R. S. J. Sparks, and S. R. Young (2002), The 26 December (Boxing Day) 1997 sector collapse and debris avalanche at Soufriere Hills Volcano, *Geol. Soc. London Mem.*, *21*, 363–407, doi:10.1144/GSL.MEM.2002.021.01.17.

Watts, P. (2000), Tsunami features of solid block underwater landslides, *J. Waterw. Port Coastal Ocean Eng.*, *126*(3), 144–152, doi:10.1061/(ASCE)0733-950X(2000)126:3(144).

Whitham, G. B. (1974), *Linear and Nonlinear Waves*, 660 pp., Wiley, New York.

Yu, B., K. Dalbey, A. Webb, M. Bursik, A. Patra, E. B. Pitman, and C. Nichita (2009), Numerical issues in computing inundation areas over natural terrains using Savage-Hutter theory, *Nat. Hazards*, *50*, 249–267, doi:10.1007/s11069-008-9336-1.

Zahibo, N., E. Pelinovsky, V. Golinko, and N. Osipenko (2006), Tsunami wave run-up on coasts of narrow bays, *Int. J. Fluid Mech. Res.*, *33*(1), 106–118, doi:10.1615/InterJFluidMechRes.v33.i1.70.

Zahibo, N., I. Didenkulova, A. Kurkin, and E. Pelinovsky (2008a), Steepness and spectrum of nonlinear deformed shallow water wave, *Ocean Eng.*, *35*(1), 47–52, doi:10.1016/j.oceaneng.2007.07.001.

Zahibo, N., E. Pelinovsky, A. Kurkin, and I. Nikolkina (2008b), Tsunami hazard for the French West Indies, Lesser Antilles, in *Integrated Coastal Zone Management*, edited by R. Krishnamurthy, pp. 517–535, Res. Publ., Singapore.

I. Nikolkina, E. Pelinovsky, T. Talipova, and N. Zahibo, Physics Department, University of the French West Indies and Guiana, 97157 Pointe-à-Pitre, Guadeloupe.